Comparison of bone SUV obtained from different SPECT/CT systems

Mana Yoshimura MD, PhD,
Natsumi Kugai MD,
Togo Aida RT,
Daisuke Hakamata RT,
Narii Miyajima RT,
Yoshitake Takahashi PhD

Department of Radiology, Tokyo Medical University, Tokyo, Japan

Keywords: Bone scintigraphy - SPECT/CT - Standardized uptake value (SUV)

Corresponding author:
Mana Yoshimura MD,
Department of Radiology, Tokyo Medical University,
6-7-1 Nishishinjuku, Shinjuku-ku,
Tokyo 160-0023, Japan
Tel.: +81-3-3342-6111 (ext. 5818),
Fax: +81-3-3348-6314
y_mana@mac.com

Received:
21 July 2023
Accepted revised:
11 October 2023

Abstract

Objective: In bone scintigraphy, it is difficult to compare quantitative values, such as standardized uptake value (SUV), obtained from 2 different single-photon emission computed tomography combined with computed tomography (SPECT/CT) devices owing to differences of imaging acquisition and analysis methods. Therefore, the purpose of this study was to compare the SUV obtained from different SPECT/CT devices using the ratio to normal bone, and to analyze the correlation between them. **Subjects and Methods:** A total of 27 prostate cancer patients who underwent bone scintigraphy either using Symbia T16 or Symbia Intevo (Siemens Medical Solutions, Erlangen, Germany) were retrospectively analyzed. In each patient, spherical voxels of interest were placed on the following 5 reference points: humeral head (humerus), femoral neck (femur), lower part of the ilium (ilium), first lumbar vertebra (L1), fifth lumbar vertebra (L5), and the maximum SUV (SUVmax) and average SUV (SUVave) of these regions were measured. **Results:** The mean and variance of SUVave (humerus) was the smallest on both SPECT/CT. To compare the SUV obtained from the 2 devices, the SUVave ratio and SUVmax ratio of each region were calculated as the SUVave and SUVmax of each region divided by the SUVave of the humeral head in each patient. Median values of the SUVmax ratio and SUVave ratio of each region showed similar tendencies in both devices, with correlation coefficients between 0.93 and 1.19. **Conclusion:** Our results demonstrated that by expressing the quantitative value of SUVave of each region as a ratio to the SUVave of the humeral head, accumulation in the targeted bone can be compared even when the imaging acquisition and analysis methods are different.

Hell J Nucl Med 2023; 26(3): 181-186 *Epub ahead of print: 14 December 2023* *Published online: 28 December 2023*

Introduction

In recent years, treatment options for prostate cancer have been increasing. Together with the advances in treatments, the role of diagnostic imaging is increasing. Namely, imaging is firstly used to accurately determine the cancer stage, secondly to assess recurrence aiming at early intervention of oligometastasis, and thirdly to evaluate the therapeutic effect of treatments to optimize the timing for switching drugs. Particularly, when prostate-specific antigen no longer reflects disease progression in patients with advanced prostate cancer, diagnostic imaging becomes the only way by which disease progression can be evaluated [1-3].

On the other hand, the evaluation of metastatic bone lesions remains difficult, although various attempts have been made to date. In 2014, the European Organization for Research and Treatment of Cancer imaging group recommended magnetic resonance imaging (MRI), that is, axial and whole-body MRI, and carbon-11 (^{11}C) or fluorine-18 (^{18}F)-choline positron emission tomography combined with computed tomography (PET/CT) as the first choice for assessing bone metastases of prostate cancer [4]. Furthermore, next-generation imaging, including anti-1-amino-3-^{18}F-fluorocyclobutane-1-carboxylic acidand gallium-68 (^{68}Ga)-prostate-specific membrane antigen were recommended in Radiographic Assessments for Detection of Advanced Recurrence III in 2019 [5]. However, these methods are not always available for clinical use.

Although the diagnostic value of conventional bone scintigraphy is rapidly decreasing, bone scintigraphy itself has made progress in 2 respects. One is that the use of SPECT or SPECT/CT imaginghas increased the detectability of small lesions. The other is that it has become possible to use the quantification of the accumulation as an imaging biomarker. There are 2 typical methods for calculating the accumulation on bone scintigraphy. The bone scan index (BSI) can be used to determine the weight ratio of the accumulation site to the whole body, using a wholebody planar image. Standardized uptake

value is the degree of local accumulation calculated using a3-dimensional image. Each index has its own strengths and weaknesses, so it is important to use them as appropriate.

In our institution, a new SPECT/CT device has been used since July 2012. As a result, the method of data acquisition and quantification has changed. Bone scan index can be calculated by BONE NAVI CAD system (FUJIFILM RI Pharma Co., Ltd., Tokyo, Japan), regardless of the imaging device or the protocol, and therefore, continuous evaluation is possible even after the SPECT/CT device has changed. On the other hand, the calculation of SUV includes many variables, and it is hence difficult to compare data when the SPECT/CT device has changed. For patients undergoing continuous treatment, changes in quantitative reference values can be a crucial problem. Therefore, in this study we compared the SUV values between 2 SPECT/CT devices using the normal bone model, and analyzed the correlation between the data.

Subjects and Methods

Patients

Data from 27patients who had undergone bone SPECT/CT imaging for metastatic prostate cancer (median age: 76years; range: 56-89 years) were retrospectively analyzed. Planar and SPECT/CT imaging was performed from the neck to the pelvis about 4h after delivering an intravenous injection of 1,003.4±102.8MBq of technetium-99m-hydroxymethylene diphosphonate (^{99m}Tc-HMDP; Nihon Medi-Physics, Tokyo, Japan) (up to June 2019) or 15.9±2.8 (range: 13.1-18.7) MBq/kg of ^{99m}Tc-methylene diphosphonate (^{99m}Tc-MDP; PD Radiopharma Inc., Tokyo, Japan) (from July 2019).

The Ethics Committee of Tokyo Medical University Hospital approved this clinical study (study approval no.:T-2021-0130). These clinical data were retrospectively analyzed, and the results did not influence any further therapeutic decision-making.

Data acquisition and reconstruction

Bone scintigraphy consisted ofsystematic planar whole-body scintigraphy (WBS) and double-bed SPECT/CT from the cervical spine to the proximal femur. Images were acquired on Symbia T16 (type-S) (until June 2019) and Symbia Intevo (type-I) (from July 2019) gamma-cameras (Siemens Healthineers, Erlangen, Germany). Both these hybrid systems incorporate a 16-slice X-ray CT scanner, and enable the acquisition of coregistered CT and SPECT images in 1 session.

Image acquisition using the type-S device

Image acquisition was performed by the standard method using low-energy high-resolution (LEHR) collimators, with an energy window of 140keV (±7.5%). Planar images were acquired with the following parameters: image matrix 256×1024, and scanning speed 16cm/min. Double-bed SPECT/CT was acquired immediately after WBS from the upper cervical spine to the proximal femur. Single photon emission computed tomography images were obtained using the following parameters: 12 seconds per step acquiring 30 projections with 180° rotation for each camera head on a 128×128-pixel matrix. Single photon emission computed tomography data were reconstructed using Flash 3D (Siemens Healthineers) with ordered subset expectation maximization (OSEM) (6 iterations, 12 subsets, and 9.6 mm Gaussian post-filtering). Computed tomography imaging consisted of the following parameters: modulated tube current intensity (CARE Dose4D algorithm, quality reference: 160mAs) 130kV, total collimation 161.2 mm, pitch 0.9, rotation time 0.6s, and was performed on the same anatomical region as SPECT.

Image acquisition using the type-I device

Acquisition was performed by the standard method using LEHR collimators, with an energy window of 140keV (±7.5%). Planar images were acquired with the following parameters: image matrix 256×1024, and scanning speed 16 cm/min. Double-bed SPECT/CT data were acquired immediately after WBS from the upper cervical spine to the proximal femora. Single photon emission computed tomography images were obtained with the following parameters: 8 seconds per step acquiring 60 projections with 180° rotation for each camera head, on a 256×256 pixel matrix. Single photon emission computed tomography data were reconstructed using xSPECT Bone and Recon Best (Siemens Healthineers), which includes a novel iterative image reconstruction algorithm, i.e., ordered subset conjugate gradient minimizer (OSCGM). Computed tomography imaging was performed with the following parameters: modulated tube current intensity (CARE Dose4D algorithm, quality reference: 160mAs) 130kV, total collimation 161.2mm, pitch 0.8, rotation time 0.6s, and was performed on the same anatomical region as SPECT.

Data analysis

In each patient, spherical voxels of interest (VOI) were placed on the following 5reference points: humeral head (humerus), femoral neck (femur), lower part of the ilium (ilium), first lumbar vertebra (L1), and fifth lumbar vertebra (L5), and SUV were measured. If metastasis or degenerative change was observed in the region, it was excluded from the measurement (Figure 1).

Analysis of data from the type-S device

Single photon emission computed tomography/CT data were analyzed using the commercially available software GI-BONE (AZE Co., Ltd., Tokyo, Japan) [6]. Using this software, slice thickness was automatically converted to about 2mm, to enable isotropic voxel evaluation. Tissue radioactivity concentrations were obtained by multiplying the SPECT counts with the Becquerel calibration factor (BCF), which was determined by scanning the cylindroid phantom filled with a known radioactivity concentration. The BCF was calculated as the ratio of actual radioactivity concentration measured by the dose calibrator in the phantom at the time of scanning (ACC) to the measured SPECT count density per scan duration(MC). That is, BCF[Bq/cps]=ACC[Bq/cc]/MC[count/cc × 1/sec]. All data were decay-corrected to the time of injection, to control fluctuations at the start time of the acquisition.

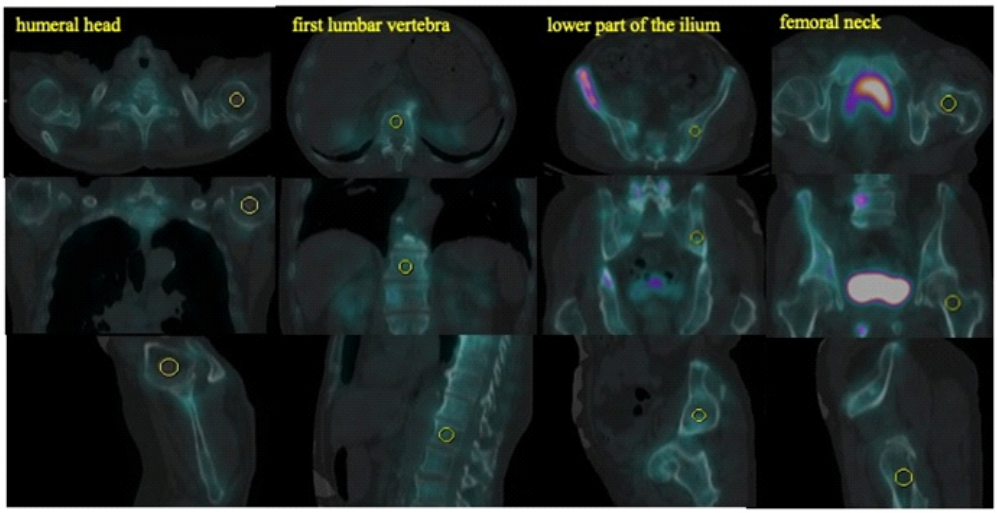

Figure 1. VOI setting by GI-BONE. Spherical voxels of interest on humeral head, first lumbar vertebra, lower part of the ilium, and femoral neck were shown.

Table 1. *Characteristics of the 2 types of devices.*

		Type-S	Type-I
Device	Model	Symbia T16 (Siemens)	SymbiaIntevo (Siemens)
	Data reconstruction	Flash 3D /OSEM	xSPECT Bone Recon Best/OSCGM
	Data analysis	GI-BONE (AZE Co.)	Advantage Workstation (GE)
Patient	Number	15	12
	Age, years (mean±SD)	73.6±8.3	72.8±8.2
Tracer	Type	^{99m}Tc-HMDP (Nihon Medi-Physics)	^{99m}Tc-MDP (PD Radiopharma Inc.)

In each patient, spherical VOI of 10pixels diameter (1.39-1.78cm^3) were placed on 5 reference points, as explained above. SUVs, such as maximum count (SUVmax) and average count (SUVave) were measured from these VOI.

Analysis of data from the type-I device

Single photon emission computed tomography/CT data were analyzed using Advantage Workstation (GE Healthcare, Japan). In each patient, spherical voxels of 1.66cm^3 were placed on 5 reference points, and SUVmax and SUVave were measured from these VOI. Table 1 shows the characteristics of the 2 types of devices.

Results

Average SUV and SUVmax were measured in 5 regions in all patients using either the type-S or type-I device. The mean and variance of SUVave of the humerus was the smallest using both devices, and we hence decided to compare each value based on each SUVave of the humerus. That is, SUVave ratio means SUVave of each region/SUVave of each humerus, and SUVmax ratio means SUVmax of each region/SUVave of each humerus. Box-and-whisker plots of these SUVave ratios and SUVmax ratios are shown in Figures 2 and 3. Median values of the SUVmax ratios and SUVave ratios of each site showed a similar tendency using both the type-S and type-I devices. Regarding region-specificitythe ratio of the ilium, L5, and L1 was high, and was scattered widely in the data obtained from both devices. Particularly using the type-I device, SUVave ratios and SUVmax ratios were scattered above the median in L5 and L1. This might be owing to the detection of the osteoblastic changes of vertebral degeneration more sensitively by the type-I device than by the type-S device.

The correlation coefficient between the SUV ratios from the type-S device with those from the type-I device was obtained using the median of the SUV ratios (Figure 4). The correlation coefficient was about 0.93 to 1.19. In other words, it may be possible to compare SUVave values obtained by the type-I device with those obtained by the type-S device, if each value is divided by SUVave of each humerus.

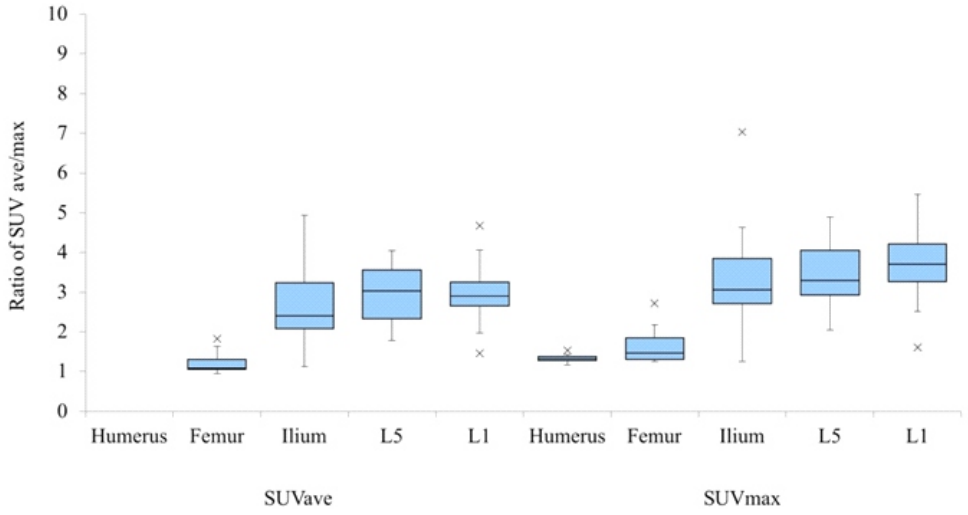

Figure 2. Box-and-whisker plots of SUVave ratio and SUVmax ratio measured using a type-S device.

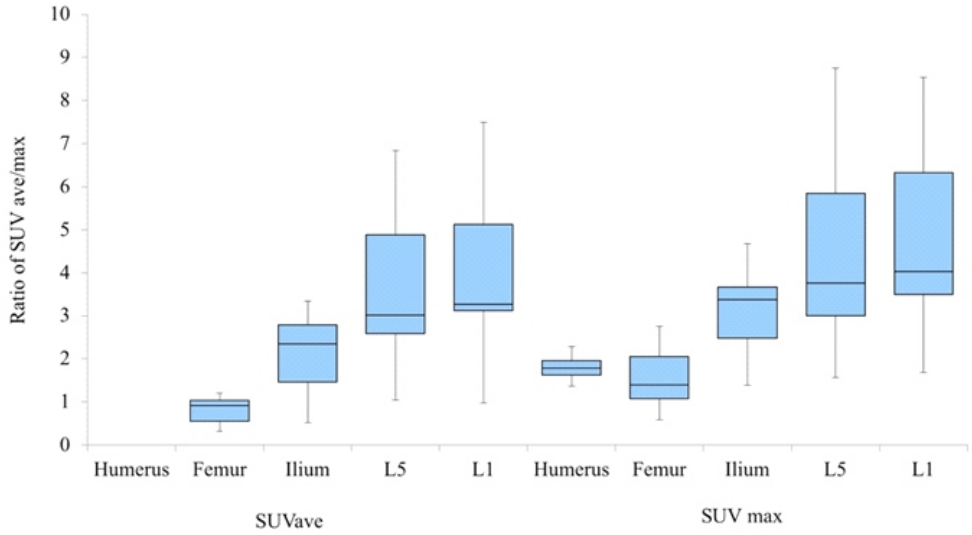

Figure 3. Box-and-whisker plots of SUVave ratio and SUVmax ratio measured using a type-I device.

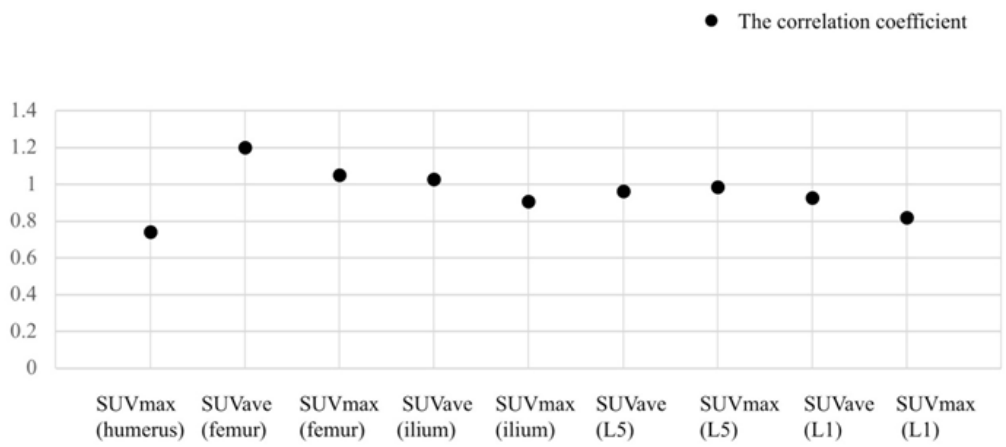

Figure 4. The correlation coefficient for SUV ratios obtained using the type-S device and those obtained using the type-I device was calculated from the median of each SUV ratio.

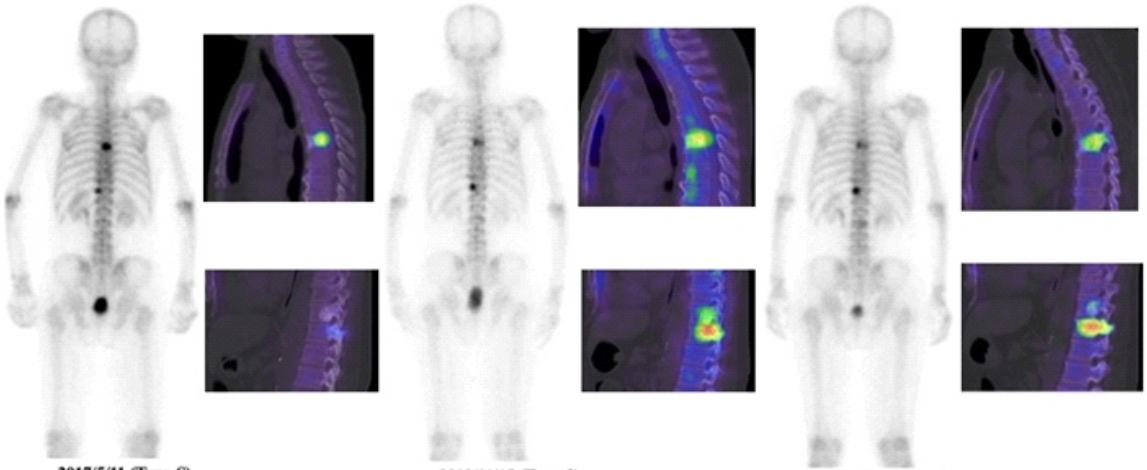

2017/5/11 (Type-S)

	SUVave	Ratio of SUVave
Humerus	1.21	
Th 6	7.07	5.84
Th 11	3.47	2.87

2018/11/15 (Type-S)

	SUVave	Ratio of SUVave
Humerus	1.14	
Th 6	3.35	2.94
Th 11	4.56	4.00

2019/8/8 (Type-I)

	SUVave	Ratio of SUVave
Humerus	4.22	
Th 6	13.06	3.09
Th 11	29.83	7.07

Figure 5. A 77-year-old male with prostate cancer. The first two bone scintigraphy was retrieved with Type-S device, and the last one with Type I. By dividing each SUVave of Th6 and Th11 by the SUVave of the humeral head respectively, the quantitative observation is available continuously. Decrease in accumulation of Th6 was confirmed by the second examination, and remained almost unchanged. On the other hand, the accumulation of Th11 increased gradually.

A case of 77-year-old male with prostate cancer was presented, whose bone metastases were followed up over time with bone scintigraphy by Type-S and Type-I devices (Figure 5).

Discussion

In recent years, the role of bone scintigraphy has changed from image evaluation of bone metabolic activity to quantitative evaluation as an imaging biomarker. There are 2 well-known indexes of bone scintigraphy, namely, BSI and SUV.

Bone scan index software is widely used and is highly versatile. The 2-dimensional distribution of bone metastases is displayed automatically or by setting an arbitrary threshold value. Many reports using BSI have already been published, particularly in the field of prostate cancer for prognosis prediction and therapeutic effect assessment [7, 8]. A major advantage of BSI is that quantitative evaluation can be performed regardless of the imaging device or protocol. Therefore, BSI data can be compared among many facilities and devices continuously. Whereas BSI displays the distribution of hypermetabolic bone, SUV displays the concentration of local bone metabolism using 3-dimensional data. Combined with volume, total bone uptake reflects the total burden of hypermetabolical lesions [9, 10]. Theoretically, SUV would more accurately reflect total bone tumor volume than BSI, but it is impractical regarding several points. Recently commercial SPECT/CT provides it's own built- in quantitative measurement system, and SUV is calculated easily and rapidly. Type-I device belongs to this category. Bone images were qualitatively and quantitatively improved when reconstructed using OSCGM-based xSPECT compared with the OSEM-based Flash 3D reconstruction. Bone SPECT/CT image reconstruction using the xSPECT algorithm is likely to provide a closer value to the true SUV [11, 12]. However, it is known that SUV itself has many bias and variance factors, such as the method of data acquisition, reconstruction, and analysis, that are performed during the calculation process. Furthermore, the methods of cross-calibration are not unified, which also causes lowering of reproducibility and stability [13]. Although harmonization and standardization among machines has been attempted, these methods are not commonly used clinically [14]. It is hence extremely difficult to compare SUV data obtained from different devices and data from various facilities.

On the other hand, general-purpose software has been developed that enables SUV calculation from SPECT/CT images that were obtained from devices that do not have such a quantitative measurement system [6]. Type-S is a device that belongs to this category. It is known that SUV values calculated by this previously used method generally result in lower values compared with SUV values obtained by the former method, and differ more greatly from the true values. However, measuring using the type-S device shows clinical usefulness as a quantitative method for follow-up or to assess therapeutic effects in the same patient.

In our present case, it was necessary to compare the quantitative values of the same patient obtained using different devices. However, owing to the characteristics of the software, SUV obtained using two different devices could not be harmonized and standardized by cross-calibration with the same phantom. However, it appears to be possible to make a simple comparison using the ratio to the humeral

head. This is because the humeral head had the most stable SUV values among data obtained from both type-S and type-I devices.

The humeral head is considered to be an area that is least susceptible to load or degenerative changes, and lesions in the humeral head can easily be set to a small VOI to evaluate only cancellous bone. Therefore, using SUV as a reference results in minimal interindividual differences. Differences in imaging acquisition, analysis methods, and drugs used were canceled by expressing the data as a ratio to the SUVave of the humeral head of each patient, with correlation coefficients between 0.93 and 1.19.

In recent years, local treatments for oligometastasis have been actively performed. In addition, the evaluation of bone metastases one by one is expected to increase further in the future. Particularly, it was shown that in treatments using radium-223 (^{223}Ra), bone scintigraphy as theranostic twins is directly associated with the therapeutic effect [15, 16]. Therefore, quantification of signal accumulation in the bones is essential for considering the indication of treatment and for assessing the therapeutic effects. There have been substantial advances in drug therapies for prostate cancer with bone metastases, but at present, treatment protocols are not standardized. Therefore, quantitative evaluation of the effects of each treatment is an urgent issue. Although calculating the true SUV is essential and necessary, it is also important to use a simple substitute value to enable the continuous assessment of therapeutic effects.

Limitations of our study include the fact that the two patient groups were not identical, the small sample size, and the retrospective design. Patients were selected as prostate cancer in their 50s to 80s. However, patients without metastases in the region of interest were retrospectively selected, which may have induced selection bias. However, our analysis provides a simple quantification method for clinical use and should be useful in the development of treatment strategies.

In conclusion, by expressing the quantitative value of SUVave of each region as a ratio to the SUVave of the humeral head, it was clarified that the accumulation measured by SPECT/CT in the targeted bone can be compared even when the imaging methods, analysis methods, and drugs used are different.

The authors declare that they have no conflicts of interest.

Bibliography

1. Yoshida S, Takahara T, Arita Y et al. Whole-body diffusion-weighted magnetic resonance imaging: Diagnosis and follow up of prostate cancer and beyond. *Int J Urol* 2021; 28: 502-13.
2. Bryce AH, Alumkal JJ, Armstrong A et al. Radiographic progression with non-rising PSA in metastatic castration-resistant prostate cancer: post hoc analysis of PREVAIL. *Prostate Cancer Prostatic Dis* 2017; 20: 221-7.
3. Bryce AH, Chen YH, Liu G et al. Patterns of cancer progression of metastatic hormone-sensitive prostate cancer in the ECOG3805 CHAARTED trial. *Eur Urol Oncol* 2020; 3: 717-24.
4. Lecouvet FE , Talbot JN , Messiou C, Bourguet et al. Monitoring the response of bone metastases to treatment with Magnetic Resonance Imaging and nuclear medicine techniques: a review and position statement by the European Organisation for Research and Treatment of Cancer imaging group. *Eur J Cancer* 2014; 50: 2519-31.
5. Crawford ED , Koo JP , Shore N et al. A Clinician's Guide to Next Generation Imaging in Patients With Advanced Prostate Cancer (RADAR III). *J Urol* 2019; 201: 682-92.
6. Kaneta T, Ogawa M, Daisaki H et al. SUVmeasurementof normal vertebrae using SPECT/CT with Tc-99m methylene diphosphonate. *Am J Nucl Med Mol Imaging* 2016; 22: 262-8.
7. Nakajima K, Mizokami A, Matsuyama H et al. Prognosis of patients with prostate cancer and bone metastasis from the Japanese Prostatic Cancer Registry of Standard Hormonal and Chemotherapy Using Bone Scan Index cohort study. *Int J Urol* 2021; 28: 955-63.
8. Ali A, Hoyle AP, Parker CC et al. The Automated Bone Scan Index as a Predictor of Response to Prostate Radiotherapy in Men with Newly Diagnosed Metastatic Prostate Cancer: An Exploratory Analysis of STAMPEDE's "M1|RT Comparison". *Eur Urol Oncol* 2020; 3: 412-49.
9. DeLaroche R, Bourhis D, Robin P et al. Feasibility Study and Preliminary Results of Prognostic Value of Bone SPECT-CT Quantitative Indices for the Response Assessment of Bone Metastatic Prostate Carcinoma to Abiraterone. *Front Med (Lausanne)* 2020; 22; 6: 342.
10. Tabotta F, Jreige M, Schaefer N et al. Quantitative bone SPECT/CT: high specificity for identification of prostate cancer bone metastases. *BMC Musculoskelet Disord* 2019; 20: 619.
11. Duncan I , Ingold N. The clinical value of xSPECT/CT Bone versus SPECT/CT. A prospective comparison of 200 scans. *Eur J Hybrid Imaging* 2018; 2: 4.
12. Miyaji N, Miwa K, Tokiwa A et al. Phantom and clinical evaluation of bone SPECT/CT image reconstruction with xSPECT algorithm. *EJNMMI Res* 2020. 10: 71.
13. Dale L Bailey, Kathy P Willowson. An Evidence-Based Review of Quantitative SPECT Imaging and Potential Clinical Applications. *J Nucl Med* 2013; 54: 83-9.
14. Nakahara T, Daisaki H, Yamamoto Y et al. Use of a digital phantom developed by QIBA for harmonizing SUVs obtained from the state-of-the-art SPECT/CT systems: a multicenter study. *EJNMMI Res* 2017; 7: 53.
15. Umeda T, Koizumi M, Fukai S et al. Evaluation of bone metastatic burden by bone SPECT/CT in metastatic prostate cancer patients: defining threshold value for total bone uptake and assessment in radium-223 treated patients. *Ann Nucl Med* 2018; 32: 105-13.
16. Owaki Y, Nakahara T, Kosaka T et al. Ra-223 SPECT for semi-quantitative analysis in comparison with Tc-99m HMDP SPECT: phantom study and initial clinical experience. *EJNMMI Res* 2017; 7: 81.